Weak ferromagnetism with very large canting in a chiral lattice: Fe(pyrimidine)$_2$Cl$_2$

R. Feyerherm* and A. Loose
Hahn-Meitner-Institut and Berlin Neutron Scattering Center, 14109 Berlin, Germany

T. Ishida and T. Nogami
Department of Applied Physics and Chemistry, The University of Electro-Communications, Chofu, Tokyo 182-8585, Japan

J. Kreitlow, D. Baabe, F. J. Litterst, S. Süllow, and H.-H. Klauss
Institut für Metallphysik und Nukleare Festkörperphysik, TU Braunschweig, 38106 Braunschweig, Germany

K. Doll
Institut für Mathematische Physik, TU Braunschweig, 38106 Braunschweig, Germany

(Received 6 February 2003; revised manuscript received 15 December 2003; published 29 April 2004)

The transition metal coordination compound Fe(pyrimidine)$_2$Cl$_2$ crystallizes in a chiral lattice, space group $I4_122$ (or $I4_322$). Combined magnetization, Mössbauer spectroscopy, and powder neutron diffraction studies reveal that it is a canted antiferromagnet below $T_N = 6.4$ K with an unusually large canting of the magnetic moments of 14° from their general antiferromagnetic alignment, one of the largest reported to date. This results in weak ferromagnetism with a ferromagnetic component of $\sim 1\ \mu_B$. The large canting is due to the interplay between the antiferromagnetic exchange interaction and the local single-ion anisotropy in the chiral lattice. The magnetically ordered structure of Fe(pyrimidine)$_2$Cl$_2$, however, is not chiral. The implications of these findings for the search of molecule based materials exhibiting chiral magnetic ordering are discussed.

DOI: 10.1103/PhysRevB.69.134427 PACS number(s): 75.25.+z, 75.50.Ee, 75.50.Xx

I. INTRODUCTION

In recent years, the interdisciplinary field of molecule based magnetic materials has been the focus of very intense research efforts.[1–5] These are directed towards synthesizing new molecular building blocks and supermolecular aggregates, which subsequently are subject to a detailed physical characterization. Here, one major issue is to develop multifunctional compounds that combine technologically relevant magnetic properties with other physical properties, such as conductivity[6] or optical activity.[7]

In this framework, extensive efforts are undertaken to find chiral magnetic materials that exhibit magnetochiral dichroism (MChD), a phenomenon first observed by Rikken and Raupach in a chiral paramagnetic material.[8] Large MChD is expected in materials that combine chirality and magnetic order. To date, however, there is no evidence for large MChD, although a number of chiral magnetic materials have been reported.[9]

Recently, the magnetism of pyrimidine bridged transition metal complexes has been investigated in which pyrimidine ($C_4H_4N_2$) plays the role of an antiferromagnetic coupling unit.[10–13] Interestingly, the halide complexes T(pyrimidine)$_2X_2$ ($T = \mathrm{Co^{II}}$, $X = \mathrm{Cl}$, Br; $T = \mathrm{Fe^{II}}$, $X = \mathrm{Cl}$) possess a chiral three-dimensional network of T ions and exhibit weak ferromagnetism below about 5 K.[14,15] The preliminary analysis of magnetization measurements on these compounds pointed to a very large canting and an associated large ferromagnetic component of the ordered moments. It appeared possible that these compounds possess a chiral magnetically ordered structure which would be of great interest in the framework of MChD.

In order to determine the magnetic structure and to elucidate the origin of the large canting we performed magnetization measurements, Mössbauer spectroscopy and powder neutron diffraction on Fe(pyrimidine)$_2$Cl$_2$. Here, we present a complete analysis of these data together with electronic structure calculations.

The basic result of our investigation is that, in spite of its chiral structure, Fe(pyrimidine)$_2$Cl$_2$ does not exhibit a chiral magnetic ordering but an exceptionally large canting of the magnetic moments of 14° from their general antiferromagnetic alignment. This canting is one of the largest reported to date. Weak ferromagnetic behavior is associated with the canting, resulting in a ferromagnetic component of 1 μ_B. We argue that in the present case the canting is due to the interplay between the antiferromagnetic exchange interaction and the local single-ion anisotropy. This implies that the chiral symmetry is the origin of the large canting in Fe(pyrimidine)$_2$Cl$_2$. We discuss the general implications of our findings for studies in search of molecule based materials exhibiting chiral magnetic ordering.

II. EXPERIMENTAL

Microcrystalline samples of Fe(pyrimidine)$_2$Cl$_2$ were obtained by mixing aqueous solutions of $\mathrm{Fe^{II}}$ chloride (e.g., 10 mmol in 20 ml H_2O) with the stoichiometric amount of pyrimidine. The resulting yellow precipitates were filtered and washed thoroughly with H_2O. Mössbauer data indicate the presence of a secondary phase, which we identified as Fe(pyrimidine)Cl$_2$. The volume amount of the secondary phase increases with storage time of the samples. While a freshly prepared sample contained less than 2% secondary phase, about 22% secondary phase have been observed in the same sample stored for three years under air (see below).

This indicates that under such conditions Fe(pyrimidine)$_2$Cl$_2$ is unstable against the formation of Fe(pyrimidine)Cl$_2$.

Magnetization measurements were carried out using an MPMS Squid magnetometer (Quantum Design). Some 20 mg of freshly prepared sample was filled into a gelatine capsule and dispersed in a small amount of mineral oil. At low temperature the oil freezes, preventing the sample grains from moving in large applied fields. Similarity of the magnetization curve for the dispersed powder sample with published data for a pure sample[15] shows that Fe(pyrimidine)$_2$Cl$_2$ does not react with the mineral oil. In contrast, dispersing Fe(pyrimidine)$_2$Cl$_2$ in ethanol leads to immediate formation of Fe(pyrimidine)Cl$_2$.

^{57}Fe Mössbauer spectroscopy experiments have been performed in a standard low-temperature Mössbauer setup at temperatures ranging from 2.3 K to 300 K [source: ^{57}Co-in-Rh matrix at room temperature; emission line half width at half maximum: 0.130(2) mm/s]. The spectra have been evaluated using the Mössbauer fitting program RECOIL[16] in the thin absorber approximation. Above T_N the spectra were modeled as Lorentzian lines in the presence of an electric-field gradient. Below T_N a diagonalization of the full hyperfine Hamiltonian including electric quadrupole and magnetic Zeeman interaction is used.[17] From the eigenvalues the energy of the resonance lines and from the eigenvectors the line intensities are obtained.

Neutron powder diffraction measurements were performed using the instruments $E6$ and $E9$ at the Berlin Neutron Scattering Center. The instrument $E6$ provides a high neutron flux and medium resolution, is equipped with a 20°-multichannel detector, and covers a range of scattering angles up to about 100° at a neutron wavelength of $\lambda = 2.448$ Å. In contrast, the instrument $E9$ is a low-flux high-resolution powder diffractometer with an extended 2θ range up to 160° and $\lambda = 1.7964$ Å. Therefore, the former was used for the study of magnetic Bragg reflections, while the latter was employed for checking the crystal structure at low temperatures. The nondeuterated sample was filled into a 7 mm diameter vanadium can with 40 mm length, resulting in a sample volume of about 1.5 cm^3. An absorption correction for cylindrical samples was applied ($\mu R = 0.94$) to account for the strong incoherent scattering from hydrogen. During the refinement, no other but symmetry constraints were used for the atom positional parameters. Therefore, the validity of the crystal structure model is proven by the correct geometry of the pyrimidine molecules determined in the refinement. The Rietveld refinement of the diffraction data was carried out using the WINPLOTR/FULLPROF package.[18]

III. RESULTS

A. Crystal structure

The high-resolution powder neutron diffraction data, taken at 10 and 298 K on a freshly prepared sample, confirm that Fe(pyrimidine)$_2$Cl$_2$ is isostructural to the Co analog for which single-crystal data are available.[19] Both compounds are tetragonal with the chiral space group no. 98, $I4_122$ (or the enantiomorphic $I4_322$). The lattice parameters for

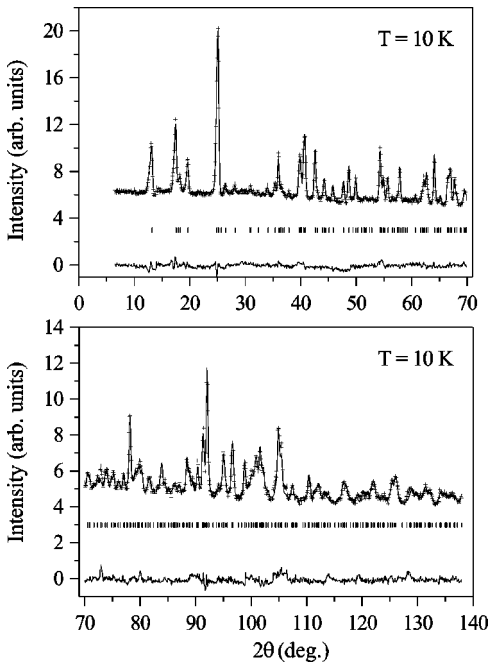

FIG. 1. High-resolution neutron powder diffractogram of Fe(pyrimidine)$_2$Cl$_2$ measured at 10 K (+). The wavelength was 1.7964 Å. The solid line through the data represents the result of a Rietveld refinement of the structural model described in the text. The difference between the measured and calculated diffractograms is shown as solid line at the bottom of each panel. Vertical bars mark expected Bragg peak positions.

Fe(pyrimidine)$_2$Cl$_2$ are $a = b = 7.3681(4)$ Å and $c = 20.339(1)$ Å at 10 K and $a = b = 7.4292(4)$ Å and $c = 20.364(1)$ Å at 298 K. At 10 K, the Fe-N and Fe-Cl distances 2.256(22) and 2.396(16) Å are determined, respectively. Due to the significantly reduced intensity of the high-angle Bragg reflections, the 298 K data are only of limited quality and therefore will not be discussed further.

Figure 1 shows the high-resolution powder diffraction pattern recorded at 10 K together with the result of the Rietveld refinement and the difference between the calculated and measured profiles. The large background signal mostly stems from the incoherent scattering from the hydrogen atoms. The thermal parameters were set equal for all atoms of the same type, because the data quality did not allow for a separate refinement for all nonequivalent atoms. The resulting crystal structure is depicted in Fig. 2 and the structural parameters are listed in Table I. No traces of any secondary phase could be identified.

The crystal structure Fe(pyrimidine)$_2$Cl$_2$ consists of a chiral three-dimensional network of Fe ions coordinated by two Cl and linked by pyrimidine molecules. Due to the 4_1 (or 4_3) screw axis, the local environment of two Fe ions in neighboring layers z and $z+1/4$ is rotated by 90°. We will discuss below that this specific feature of the crystal structure of Fe(pyrimidine)$_2$Cl$_2$ can be regarded as the origin of the large canting observed in the magnetically ordered state.

In the local FeN$_4$Cl$_2$ geometry all nitrogen atoms of pyrimidine are equatorially coordinated. It was pointed out[13]

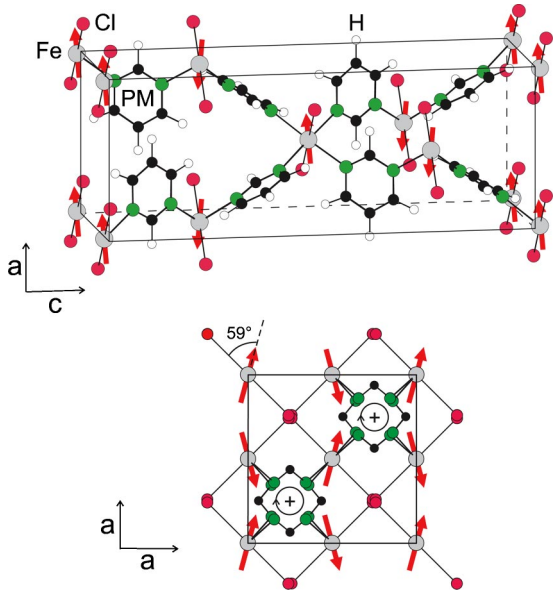

FIG. 2. The crystal and magnetic structure of Fe(pyrimidine)$_2$Cl$_2$. Lower section: A view along the c axis, with the positions of the 90° screw axes marked. The angle $\alpha = 59°$ between the magnetic moments and the local electric-field gradient is also indicated (see text).

that in this case antiferromagnetic correlations are expected to be transferred through the pyrimidine molecule.

B. Magnetization

Figure 3 depicts the M vs H hysteresis curve of a freshly prepared sample Fe(pyrimidine)$_2$Cl$_2$ measured at 1.8 K. On increasing the field from zero, we observe an initial steep increase of the magnetization in a low field region (a few 100 Oe) to a value much smaller than the full Fe^{II} moment. Subsequently, a rounded crossover around 500 Oe is followed by an almost linear field dependence up to 55 kOe. On sweeping the field down from 55 kOe, a weak hysteresis develops and

TABLE I. Structural parameters of Fe(pyrimidine)$_2$Cl$_2$ at 10 K, slightly above the magnetic transition. Space group $I4_122$ (no. 98), $a = b = 7.3681(4)$ Å, $c = 20.339(1)$ Å. The occupancy is unity for all atoms. Quality of the refinement: $R_p = 2.3\%$, $R_{wp} = 3.2\%$, $R_{expected} = 1.4\%$.

Atom[a]	x/a	y/b	z/c	B (Å^2)
Fe ($4b$)	0	0	0	0.4(1)
Cl ($8d$)	0.229(2)	−0.229(2)	0	0.2(1)
N ($16g$)	0.150(2)	0.165(2)	0.076(1)	0.3(1)
C1 ($8f$)	0.066(3)	1/4	1/8	0.3(1)
C2 ($16g$)	0.337(3)	0.168(3)	0.075(1)	0.3
C3 ($8f$)	0.431(3)	1/4	1/8	0.3
H1 ($8f$)	−0.087(7)	1/4	1/8	1.4(2)
H2 ($16g$)	0.393(5)	0.108(5)	0.032(2)	1.4
H3 ($8f$)	0.579(7)	1/4	1/8	1.4

[a]Multiplicity and Wykoff letter.

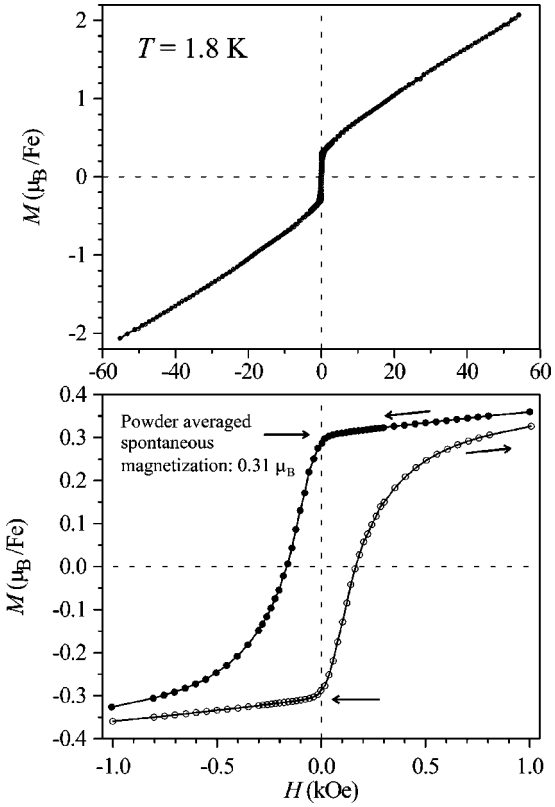

FIG. 3. Hysteresis loop of Fe(pyrimidine)$_2$Cl$_2$ measured at 1.8 K; (a) full hysteresis curve; (b) a blow-up of the low-field section.

a sharp kink is observed around $H = 0$. Upon increasing temperature the hysteresis in the $M(H)$ curves is reduced and vanishes above 6.4 K.

This behavior is typical for a weak ferromagnet, where the steep increase at low H reflects the spontaneous magnetization and the linear high-field behavior is due to the dominant antiferromagnetic interactions. The kink around $H = 0$ allows for an accurate determination of the spontaneous magnetization. We obtain a value of 0.31(1) μ_B on the powder average at 1.8 K. The coercitive field is small (~150 Oe), classifying Fe(pyrimidine)$_2$Cl$_2$ as a soft magnet.

Assuming that the ferromagnetic component in a given magnetic domain is pointing along a specific crystal direction, the measured powder average of the spontaneous magnetization has to be multiplied by a factor of three to obtain the ferromagnetic moment along this axis. Then, from the magnetization we obtain a ferromagnetic component of 0.93(3) μ_B per Fe ion in the canted antiferromagnetic state. We will show in the following that this value is in full agreement with the combined Mössbauer spectroscopy and neutron diffraction results.

C. Mössbauer spectroscopy

In Fig. 4 we plot the Mössbauer spectra of Fe(pyrimidine)$_2$Cl$_2$ at temperatures 2.3–300 K. In Fig. 4(a) data are shown for a newly made sample, while in Fig. 4(b) we display the spectra taken on the same sample after storage for two years under air.

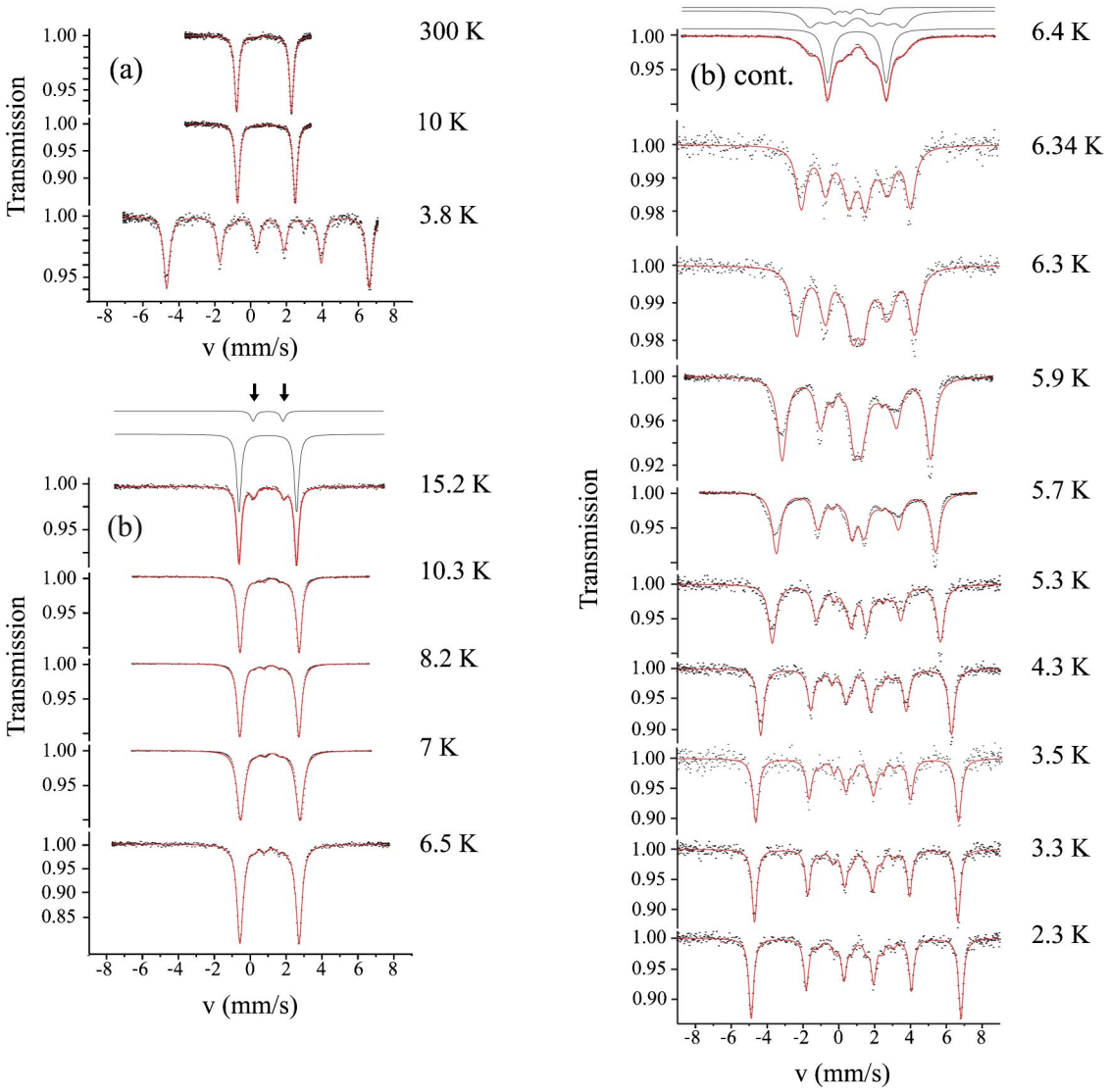

FIG. 4. Mössbauer spectra of Fe(pyrimidine)$_2$Cl$_2$ measured at various temperatures. The solid lines are fits to the data points. The data sets (a) and (b) were measured after different storage times of the sample, arrows in the left part of (b) mark the contribution from a secondary phase (for details see text).

At room temperature, for the newly made sample we observe a two line spectrum, resulting from a quadrupole splitting of $QS=3.11(1)$ mm/s and an isomer shift of $IS=1.03(1)$ mm/s (relative to α-iron foil) [Fig. 4(a) and Table II]. These are typical values for high spin Fe^{II}.[20] Upon lowering the temperature, and above T_N, both QS and IS slightly increase.

Below T_N, at 3.8 K, for the newly made sample eight separate absorption lines with an irregular intensity distribution are observed. As demonstrated by Kündig,[21] such spectra arise from the coexistence of an electric-field gradient and a hyperfine magnetic field (B_{HF}) at the Fe nucleus, whose main axes span an angle α. A fit to the data at 3.8 K based on the diagonalization of the full hyperfine Hamiltonian including electric quadrupole and magnetic Zeeman interaction as described in Ref. 21 yields values for the isomer shift $IS=1.16(1)$ mm/s, quadrupole splitting $QS=3.28(1)$ mm/s, asymmetry parameter $\eta=(V_{xx}-V_{yy})/V_{zz}=0.11(1)$, and the magnetic hyperfine field $B_{HF}=30.2(1)$ T. Moreover, from the fit we determine the angle α between the direction of the hyperfine magnetic field, B_{HF}, and the main electric field gradient component V_{zz} to 59(1)°.

After storage of the sample for two years under air we observe an additional two line spectrum resulting from quadrupole splitting of a secondary phase [arrows in Fig. 4(b) for 15.2 K]. We have chemically isolated this secondary phase and characterized it as Fe(pyrimidine)Cl$_2$.[22] A Mössbauer study above 11 K on a single phase sample of this secondary phase reveals that it can be taken into account in a fit of the data on Fe(pyrimidine)$_2$Cl$_2$ using a quadrupole split set of lines with $QS=1.73(1)$ mm/s and $IS=1.21(1)$ mm/s. In Fig. 4(b) we illustrate the decomposition of the data into two components for the spectrum at 15.2 K by including the separate absorption lines for the two chemical phases. From

TABLE II. Refined parameters from the Mössbauer spectra on Fe(pyrimidine)$_2$Cl$_2$ between 300 and 2.3 K for the newly made sample (**A**) and after storage for two years (**B**). Parameters are the isomer shift IS, quadrupole splitting QS and below T_N the hyperfine field B_{HF}, asymmetry parameter η and canting angle α, with χ^2 as measure for the fit quality.

T (K)	IS [mm/s]	QS [mm/s]	η [ ]	B_{HF} [T]	α [°]	χ^2
A						
300	1.03(1)	3.11(1)	0	0	0	1.07
10.4	1.16(1)	3.27(1)	0	0	0	1.17
3.8	1.16(1)	3.28(1)	0.11(1)	30.2(1)	59(1)	1.35
B						
15.2	1.16(1)	3.28(1)	0	0	0	1.47
10.3	1.16(1)	3.27(1)	0	0	0	4.7
8.2	1.16(1)	3.28(1)	0	0	0	8.5
7	1.18(1)	3.37(1)	0	0	0	27
6.5	1.16(1)	3.30(1)	0	0	0	1.19
6.4[b]	1.16(1)	3.34(1)	0	0	0	3.5
6.4[b]	1.16(1)	3.36(1)	0.1[a]	7.7(1)	59[a]	3.5
6.34	1.14(1)	3.30(3)	0.08(5)	11.5(1)	60(1)	1.19
6.3	1.14(1)	3.29(2)	0.09(5)	13.3(1)	59(1)	1.53
5.9	1.16 [a]	3.26(1)	0.10[a]	19.7(1)	60(1)	13
5.7	1.16 [a]	3.31(1)	0.08(3)	21.7(1)	60(1)	39
5.3	1.14(1)	3.33(2)	0.06(3)	23.4(1)	59(1)	1.73
4.3	1.15(1)	3.23(1)	0.10(1)	28.1(1)	59(1)	1.54
3.5	1.16(1)	3.25(3)	0.11(1)	30.2(1)	60(1)	1.06
3.3	1.16(1)	3.32(1)	0.10(1)	30.3(1)	59(1)	1.24
2.3	1.16(1)	3.33(1)	0.10(1)	31.5(1)	59(1)	1.01

[a]Parameters fixed to stabilize fit.

[b]Spectrum at 6.4 K has been fitted assuming 50% antiferromagnetically ordered and 50% paramagnetic sample volume.

this procedure, the relative spectral weight of the secondary phase is estimated to 14%. It increases to 22% after three year storage.

The secondary phase exhibits magnetic long range order below 11 K. Mössbauer spectra on Fe(pyrimidine)Cl$_2$ measured between 2.5 and 9 K are successfully reproduced by the full hyperfine Hamiltonian with nearly temperature independent hyperfine parameters.[22] Therefore, the parameter set evaluated at 3 K for Fe(pyrimidine)Cl$_2$ was used to describe the secondary phase signal in the measurements on Fe(pyrimidine)$_2$Cl$_2$ at 8.2 K and below. This way, we evaluate the T dependence of the parameters IS, QS, η, B_{HF}, and α for Fe(pyrimidine)$_2$Cl$_2$. The resulting fits and fit parameters are included in Fig. 4(b) and Table II, respectively.

With our procedure, we nicely reproduce the spectra on Fe(pyrimidine)$_2$Cl$_2$ at temperatures down to T_N as well as at 5.3 K and below [Fig. 4(b)]. The mismatch between fit and data in the range from T_N down to $\sim$5.7 K reflects a distribution of the transition temperature T_N of the main phase Fe(pyrimidine)$_2$Cl$_2$. This is demonstrated for the spectrum taken at 6.4 K. Here, we had to assume that 50% of the main phase volume is paramagnetic and 50% antiferromagnetically ordered. The corresponding data decomposition of the full spectrum into the three components, one from paramagnetic and a second from antiferromagnetic Fe(pyrimidine)$_2$Cl$_2$, plus a third from the secondary phase, is exemplified in Fig. 4(b).

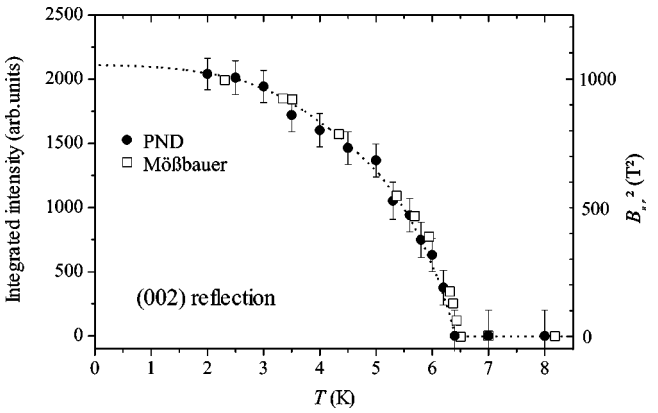

FIG. 5. Temperature dependence of the square of the hyperfine field B_{HF} observed by Mössbauer spectroscopy (data set *B* of Table II), together with the integrated intensity of the (002) Bragg reflection, being proportional to the square of the ordered moment. The dashed line is a guide to the eye.

In consequence, fits of our Mössbauer spectra assuming a homogeneous antiferromagnetically ordered sample properly reproduce the data well only as long as the hyperfine field B_{HF} does not vary rapidly with temperature, i.e., sufficiently far below T_N. In contrast, close to T_N the distribution of the local hyperfine fields B_{HF} causes a larger mismatch between fit and data. These issues in mind, we find that within experimental resolution IS, QS, η, and α are temperature independent below T_N. The temperature dependence of B_{HF}^2 is displayed in Fig. 5. B_{HF}^2 vanishes at $T_N \sim 6.4$ K and exhibits a behavior typical for a magnetic second-order transition.

To derive the spatial orientation of the magnetic moment at the Fe site from the knowledge of α, one needs to know the orientation of V_{zz} with respect to the crystal lattice. Since this cannot be determined experimentally from Mössbauer experiments on a polycrystalline sample we performed electronic structure calculations as described in the following section.

D. Theoretical calculations

Electronic structure calculations were performed with a code based on a local basis set.[23] Unrestricted Hartree-Fock and density-functional calculations were performed for the periodic system. The functional was chosen as a hybrid functional with a mixture of Fock exchange, a modification of the Becke gradient corrected exchange functional, the Vosko-Wilk-Nusair local correlation functional, and the gradient corrected correlation potential by Lee, Yang, and Parr. This combination has become one of the most popular density functionals and is usually referred to as B3LYP.[24]

The basis functions were chosen as Gaussian type orbitals. The iron basis set[25] (outermost *d*-exponent 0.4345) is of the size $[5s4p2d]$, the chlorine basis set[26] (with one *d* exponent with value 0.5) of the size $[5s4p1d]$, carbon and nitrogen basis sets[27] of the size $[3s2p1d]$, and finally a

$[2s1p]$ hydrogen basis set[28] was used. To test the stability of the results, additional tight basis functions were added for the iron atoms and a diffuse sp function (exponent 0.12) was added at the nitrogen site to account for a better description of this negatively charged atom. The results were, however, found to be essentially stable with respect to the various basis sets. With these parameters, the Hartree-Fock or Kohn-Sham equations for the antiferromagnetic (Néel-like) structure are solved self-consistently, and properties such as charge distributions and field gradients can be computed. The structural data used in the calculations are taken from Table I.

From the calculations, the charges were determined to be $+1.9$ for Fe, -1.0 for Cl, -0.8 for N, between 0 and $+0.7$ for carbon, while the hydrogen atoms were found to be slightly positive charged (at most $+0.1$). The spin on the Fe site is 1.9, with a corresponding magnetic moment of 4.0 μ_B, using a g factor of 2.13.[15] Thus, there is moment reduction by about 5% due to covalency effects. The magnitude of the spin at the Cl, N, or C sites is less than 0.1 and thus negligible, the spin at the hydrogen sites virtually zero. The electric field gradient at the Fe site has components with the value $V_{xx}=-0.8$, $V_{yy}=-1.3$, and $V_{zz}=2.1\times10^{22}$ V/m^2. These numbers have an uncertainty of the order of 0.1×10^{22} V/m^2. The asymmetry parameter η is especially sensitive to this uncertainty and values in the range from 0.1 to 0.3 are obtained.

The second largest component of the tensor is identical with the crystallographic c direction, the other two components lie perpendicular in the tetragonal basal plane and are rotated by $\pm45°$ with respect to the a axis. The largest component of the tensor points into the direction of the Cl atoms. Therefore, the Fe-Cl bonds define the principal axis of the electric-field gradient measured in the Mössbauer spectroscopy experiments.

We compare the computed field gradient with the experimental value obtained from Mössbauer spectroscopy by converting according to the formula $QS=eQV_{zz}c/2E_0$, with $E_0=14.4$ keV and using the value of 0.16 barn for the quadrupole moment Q.[29] With these parameters, we obtain a computed $QS=3.5$ mm/s which is in good agreement with the experimental value.

E. Magnetic structure

In Fig. 6 we display the powder neutron diffractograms taken at 1.6 and 7 K (i.e., well below and above T_N), as well as the difference of these two diffractograms, measured on a freshly prepared sample (same sample as used for the crystal structure determination, Sec. III A). The Rietveld refinement of these data was performed, using the positional parameters, thermal factors and lattice constants from Table I, i.e., from the separate high-resolution diffraction experiment at 10 K. The only free parameters were line shape, background and scaling parameters. No additional structural information is obtained. There is no indication for any thermal variation of the structural parameters between 1.6 and 10 K.

The difference spectrum reveals additional Bragg intensities produced by the long-range magnetic ordering. All magnetic reflections can be indexed on the basis of the crystallographic unit cell. The rule $h+k+l=$ even for the observed magnetic Bragg reflections (hkl) indicates that in the magnetically ordered phase the body centering is conserved. A number of observed magnetic Bragg reflections, namely, (002), (110), (114), and (202), break the selection rules for the special position of Fe and therefore cannot be related to any ferromagnetic component. In contrast, all observed magnetic Bragg reflections, but a possible (112), can be reproduced assuming a simple antiferromagnetic ordering between moments in neighboring layers z and $z+1/4$. The presence and strength of the reflection (002) suggest that the magnetic moments lie perpendicular to the c axis.

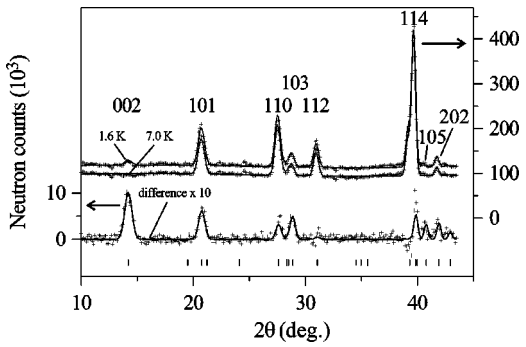

FIG. 6. The two neutron powder diffractograms measured at 1.6 K (below T_N) and 7.0 K (above T_N) for Fe(pyrimidine)$_2$Cl$_2$, offset for clarity, and the difference of the two diffractograms. The wavelength was 2.448 Å. The reflections are indexed on the basis of the crystallographic unit cell. The Rietveld refinements of all three data sets are shown as lines through the corresponding data points.

Initial refinements of the 1.6 K data based on a simple antiferromagnetic structure showed already good agreement and resulted in an ordered moment of roughly 4 μ_B.[15] However, the orientation of the moments within the basal plane as well as the angle and direction of canting can not be determined from these data. We wish to point out that the only unambiguous signature of the ferromagnetic component is the weak additional magnetic intensity expected at the (112) position, which, however, is hidden in the noise of the experimental data. We therefore use the information from the Mössbauer spectroscopy to arrive at the final magnetic structure model.

With the principal axis of the electric-field gradient parallel to the Fe-Cl bonds, as it was determined in the theoretical calculations, in the basic antiferromagnetic structure the moments have to be aligned parallel to the a axis in order to enclose an identical angle with the local electric-field gradient at each Fe. To increase this angle from 45° to 59°—as observed in the Mössbauer experiment—either a canting by 14° within the basal plane (along a') or by 45° along c needs to be introduced. However, only a canting in the basal plane gives a ferromagnetic component close to 1 μ_B, whereas a canting along c would require a ferromagnetic component of 2.8 μ_B. Comparing these values to the results from the magnetization measurements, the latter model can be ruled out. Therefore, for the final magnetic structure model, the moments were confined to the basal plane and the canting angle 14° was fixed. The fit of this final model to the

difference spectrum is shown in Fig. 6 as solid line. In this fit, the only free parameter is the magnitude of the ordered moment. All other parameters, such as lattice constants and line shapes, are fixed by the Rietveld refinements of the high-resolution diffraction data and of the low-resolution nuclear Bragg pattern recorded at 7 K.

In view of the large background noise from the hydrogen incoherent scattering, the refinement gives good agreement with the data ($R_p=0.114$, $R_{wp}=0.137$, $R_{expected}=0.118$ referring to the difference diffractogram). The fit yields an ordered moment of 4.0(3) μ_B—in agreement with the above calculated full moment on the Fe—and a ferromagnetic component of 1.0(1) μ_B. The latter value is in good agreement with the magnetization data discussed above, which resulted in a ferromagnetic component of 0.93(3) μ_B per Fe ion in the canted antiferromagnetic state.

The magnetic ordering breaks the symmetry of the lattice. The 90° screw axis symmetry is lifted as well as the tetragonal symmetry—the two basal-plane axes become nonequivalent. The magnetic structure can be represented in a two-sublattice model with the magnetic space group $I112'$ (special cell choice of space group $C2$ with c as unique axis) with one sublattice at (0,0,0) and the second at (1/2,0,1/4).

The temperature dependence of the integrated intensity of the (002) Bragg reflection is included in Fig. 5. With a temperature independent canting angle α from the Mössbauer study, the Bragg intensity is proportional to the square of the ordered moment, and thus to the hyperfine field B_{HF}^2. Figure 5 reveals a very good agreement between the T dependence of B_{HF}^2 and of the magnetic Bragg intensity in Fe(pyrimidine)$_2$Cl$_2$, thus verifying the validity of our Mössbauer and neutron diffraction analysis. The quantities represent the temperature dependence of the antiferromagnetic order parameter, decreasing continuously with rising temperature and vanishing at $T_N=6.4(2)$ K.

IV. DISCUSSION

The canting angle $\alpha=59°-45°=14°$ observed in the present measurements is extremely large, actually one of the largest reported to date for any weak ferromagnetic compound. For example, weak ferromagnetism of Fe with a canting angle of 16° has been reported for the intermetallic compound UFe_4Al_8. However, the ferromagnetic component is only 0.3 μ_B per Fe in this compound and the canting is due to an interaction between the U 5f and the Fe 3d electrons.[30] Therefore, the physics of this compound is hardly comparable to that of Fe(pyrimidine)$_2$Cl$_2$.

Large canting angles of 2°–7° have been also observed in Gd_2CuO_4-type cuprates. For these materials, a correlation between weak ferromagnetism and the crystal symmetry has been discussed in detail.[31] We believe that such a correlation is also present in Fe(pyrimidine)$_2$Cl$_2$ and that the large canting observed in this compound is a direct result of its chiral lattice symmetry. Due to this symmetry, the orientation of the local easy axis varies by 90° between nearest Fe neighbors linked by a pyrimidine molecule. Therefore, the local anisotropy would favor a 90° alignment between the moments. However, the AFM interaction favors a 180° alignment. The actual angle $180°-2\alpha=152°$ between neighboring moments therefore can be regarded as the result of the competition of the local anisotropy and the antiferromagnetic exchange. The final magnetic structure model suggests that the local easy axis lies perpendicular to c and within the equatorial plane of the local coordination octahedron of each Fe. Thus, it coincides with the axis of the smallest electric field gradient component V_{xx} calculated above. We may express this anisotropy as an additional term in the Hamiltonian of the system,

$$\mathbf{H}=\sum_{NN}\left[J\vec{S}_1\cdot\vec{S}_2+D(S_{1x}S_{2y})\right], \tag{1}$$

where the sum is over all pairs of nearest-neighbor spins $(\vec{S}_1,\vec{S}_2)$, $\vec{S}_j=(S_{jx},S_{jy},S_{jz})$, and $D<0$. The resulting angle α is related to D and J by $D/J=-2\sin 2\alpha$. With the measured α we get $D=-0.96J$. If one would assign the canting to a Dzyaloshinsky-Moriya type interaction,[32–34] the Dzyaloshinsky-Moriya vector was aligned along c as expected for symmetry reasons and the Dzyaloshinsky-Moriya term would read $D(S_{1x}S_{2y}-S_{1y}S_{2x})$. The latter term of (1) differs from the Dzyaloshinsky-Moriya term in leading to a canting towards specific axes x and y for S_1 and S_2, respectively, rather than a canting within the tetragonal basal plane in general.

It is interesting to note that magnetization data on the Co analogs of the present compound, Co(pyrimidine)$_2$Cl$_2$ and Co(pyrimidine)$_2$Br$_2$,[14] indicate even larger ferromagnetic components and therefore suggest even larger canting angles than in Fe(pyrimidine)$_2$Cl$_2$. Another example of such a large canting may be 3D-[Fe(N$_3$)$_2$(4,4′-bpy)], with bpy =4,4′-bipyridine. A microcrystalline sample of this compound was recently reported to exhibit a large spontaneous magnetization of 0.48 μ_B per Fe tentatively ascribed to ferromagnetic ordering while a canted structure was not excluded.[35,36] This tetragonal compound also forms a chiral 3D network structure, space group $P4_12_12$, which is closely related to that of Fe(pyrimidine)$_2$Cl$_2$. The negative Curie-Weiss temperature and the similarity of the magnetization data of 3D-[Fe(N$_3$)$_2$(4,4′-bpy)] with that of the T(pyrimidine)$_2X_2$ complexes suggests that also in the former a canted antiferromagnetic state with a very large canting (of roughly 20°) within the tetragonal basal plane is realized.

To our knowledge, only few other molecule based magnets with chiral crystal structures have been reported. The oxalato (ox) based compound [Co(2,2′-bpy)$_3$][Co$_2$(ox)$_3$]ClO$_4$ (Ref. 37) exhibits weak ferromagnetism with small canting ($\mu_{\mathrm{fm}}=0.009\ \mu_B$). The compounds of the series [Z$^{\mathrm{II}}$(2,2′-bpy)$_3$][ClO$_4$][M$^{\mathrm{II}}$Cr$^{\mathrm{III}}$(ox)$_3$][38] order ferromagnetically. Both systems crystallize in the cubic chiral space group $P4_132$. Another example is ferrimagnetic Mn(hfac)$_2$NITPhOMe, crystallizing in space group $P3_1$.[39] The other compounds discussed in the framework of chiral magnetism are based on chiral constituents and crystallize in noncentrosymmetric but achiral space groups, such as $P1$ or $P2_12_12_1$.[9]

V. CONCLUSION

We have shown that Fe(pyrimidine)$_2$Cl$_2$ is a weak ferromagnet with low coercitive field but a very large ferromagnetic component of $\sim 1\ \mu_B$, corresponding to a canting angle of 14°. This is one of the largest values reported to date. In a given magnetic domain, the antiferromagnetic component of the moments is confined to the *a* axis, while the canting occurs along the perpendicular direction a'. We argued that the large canting in Fe(pyrimidine)$_2$Cl$_2$ is the direct result of its chiral lattice symmetry leading to a competition between the antiferromagnetic exchange interaction and the local single-ion anisotropy. The appearance of canting rather than a chiral magnetic structure may be a general feature of the magnetic ordering in similar structures possessing 90° screw axes. This observation is of interest in view of the extensive efforts to produce a molecular magnet exhibiting chiral magnetic ordering. To date, both strategies, crystallizing (i) achiral constituents in a chiral lattice and (ii) chiral constituents in non-centrosymmetric but achiral lattices did not lead to chiral magnetic ordering.

Most of these compounds possess 90° or 180° screw axes. These lead to a $\pm 90°$ or to no alteration at all, respectively, of the local anisotropy along the screw axes and thus do not necessarily support any chirality of the ordered magnetic structure. Local anisotropy supporting chiral magnetic ordering therefore appears more likely in chiral trigonal/hexagonal lattices. We suggest that the search for chiral magnetic ordering should focus on compounds of that kind.

ACKNOWLEDGMENTS

We thank N. Stüsser and D. Toebbens for experimental support. This work has been partially supported by the Deutsche Forschungsgemeinschaft DFG under Contract No. SU229/6-1.

*Electronic address: Feyerherm@hmi.de

[1] M. Verdaguer, Polyhedron **20**, 1115 (2001), and the following articles of Issues 11–14 of this volume (Proc. ICMM 2000, San Antonio).
[2] E. Coronado Miralles, Polyhedron **22**, 1725 (2003), and the following articles of Issues 14–17 of this volume (Proc. ICMM 2002, Valencia).
[3] O. Kahn, *Molecular Magnetism* (VCH, New York, 1993).
[4] J. Miller and A. Epstein, Angew. Chem., Int. Ed. Engl. **33**, 385 (1994).
[5] D. Gatteschi, Adv. Mater. (Weinheim, Ger.) **6**, 635 (1994).
[6] E. Coronado, J.P. Galán-Mascarós, C.J. Gómez-García, and V. Laukhin, Nature (London) **408**, 447 (2000).
[7] S. Benard, P. Yu, J. Rivière, R. Clément, J. Guilhelm, L. Tchernatov, and K. Nakatani, J. Am. Chem. Soc. **122**, 9444 (2000).
[8] G.L.J.A. Rikken and E. Raupach, Nature (London) **390**, 493 (1997).
[9] E. Coronado, C.J. Gómez-García, A. Nuez, F.M. Romero, E. Rusanov, and H. Stoeckli-Evans, Inorg. Chem. **41**, 4615 (2002), and references therein.
[10] T. Ishida, S.-I. Mitsubori, T. Nogami, and H. Iwamura, Mol. Cryst. Liq. Cryst. **233**, 345 (1993).
[11] G.D. Munno, T. Poerio, M. Julve, F. Lloret, and G. Viau, New J. Chem. **22**, 299 (1998).
[12] R. Feyerherm, S. Abens, D. Günther, T. Ishida, M. Meißner, M. Meschke, and T. Nogami, J. Phys.: Condens. Matter **39**, 8495 (2000).
[13] F. Mohri, K. Yoshizawa, T. Yamabe, T. Ishida, and T. Nogami, Mol. Eng. **8**, 357 (1999).
[14] K. Nakayama, T. Ishida, R. Takayama, D. Hashizume, M. Yasui, F. Iwasaki, and T. Nogami, Chem. Lett. **27**, 497 (1998).
[15] K. Zusai, T. Kusaka, T. Ishida, R. Feyerherm, M. Steiner, and T. Nogami, Mol. Cryst. Liq. Cryst. Sci. Technol., Sect. A **343**, 127 (2000).
[16] K. Lagarec, *Reoil*, Version 1.02 (Department of Physics, University of Ottawa, Ottawa, 1998).
[17] N. Blaes, H. Fischer, and U. Gonser, Nucl. Instrum. Methods Phys. Res. B **9**, 201 (1985).
[18] T. Roisnel and J. Rodríguez-Carvajal, Mater. Sci. Forum **378-381**, 118 (2001).
[19] D. Hashizume, R. Takayama, K. Nakayama, T. Ishida, T. Nogami, M. Yasui, and F. Iwasaki, Acta Crystallogr., Sect. C: Cryst. Struct. Commun. **55**, 1793 (1999).
[20] D. Barb, *Grundlagen und Anwendungen der Mössbauerspektroskopie* (Akademie, Berlin, 1980).
[21] W. Kündig, Nucl. Instrum. Methods **48**, 219 (1967).
[22] R. Feyerherm *et al.* (2003), a full account of the properties of this material will be given elsewhere.
[23] V.R. Saunders, R. Dovesi, C. Roetti, M. Causá, N.M. Harrison, R. Orlando, and C.M. Zicovich-Wilson, CRYSTAL98 *User's Manual* (University of Torino, Torino, Italy, 1998).
[24] P.J. Stephens, F.J. Devlin, C.F. Chabalowski, and M.J. Frisch, J. Phys. Chem. **98**, 11623 (1994).
[25] M. Catti, G. Valerio, and R. Dovesi, Phys. Rev. B **51**, 7441 (1995).
[26] M. Prencipe, A. Zupan, R. Dovesi, E. Aprá, and V.R. Saunders, Phys. Rev. B **51**, 3391 (1995).
[27] R. Dovesi, M. Causá, R. Orlando, C. Roetti, and V.R. Saunders, J. Chem. Phys. **92**, 7402 (1990).
[28] R. Ditchfield, W.J. Hehre, and J.A. Pople, J. Chem. Phys. **54**, 724 (1971).
[29] P. Dufek, P. Blaha, and K. Schwarz, Phys. Rev. Lett. **75**, 3545 (1995).
[30] J.A. Paixão, B. Lebech, A.P. Gonçalves, P.J. Brown, G.H. Lander, P. Burlet, A. Delapalme, and J.C. Spirlet, Phys. Rev. B **55**, 14 370 (1997).
[31] H.M. Luo, Y.Y. Hsu, B.N. Lin, P. Chi, T.J. Lee, and H.C. Ku, Phys. Rev. B **60**, 13 119 (1999).
[32] I. Dzyaloshinsky, J. Phys. Chem. Solids **4**, 241 (1958).
[33] T. Moriya, Phys. Rev. **117**, 635 (1960).
[34] T. Moriya, Phys. Rev. **120**, 91 (1960).
[35] T. Yuen, C.L. Lin, A. Fu, and J. Li, J. Appl. Phys. **91**, 7385 (2002).
[36] A. Fu, X. Huang, J. Li, T. Yuen, and C.L. Lin, Chem.-Eur. J. **8**, 2239 (2002).
[37] M. Hernández-Molina, F. Lloret, C. Ruiz-Pérez, and M. Julve, Inorg. Chem. **37**, 4131 (1998).
[38] E. Coronado, J.P. Galán-Mascarós, C.J. Gómez-García, and J.M. Martínez-Agudo, Inorg. Chem. **40**, 113 (2001).
[39] A. Caneschi, D. Gatteschi, P. Rey, and R. Sessoli, Inorg. Chem. **30**, 3936 (1991).